

Movable Antenna Enhanced NOMA Short-Packet Transmission

Xinyuan He, Wen Chen, *Senior Member, IEEE*, Qingqing Wu, *Senior Member, IEEE*, Xusheng Zhu, and Nan Cheng, *Senior Member, IEEE*

Abstract—This letter investigates a short-packet downlink transmission system using non-orthogonal multiple access (NOMA) enhanced via movable antenna (MA). We focus on maximizing the effective throughput for a core user while ensuring reliable communication for an edge user by optimizing the MAs' coordinates and the power and rate allocations from the access point (AP). The optimization challenge is approached by decomposing it into two subproblems, utilizing successive convex approximation (SCA) to handle the highly non-concave nature of channel gains. Numerical results confirm that the proposed solution offers substantial improvements in effective throughput compared to NOMA short-packet communication with fixed position antennas (FPAs).

Index Terms—Movable antenna (MA), Non-orthogonal multiple access (NOMA), short-packet communication.

I. INTRODUCTION

IN the era of the Internet of Things (IoT), the necessity for low-latency communication has become increasingly pronounced, owing to its pivotal role across a spectrum of application domains [1]. In industrial automation, seamless coordination and real-time responsiveness are paramount, low-latency communication ensures the smooth operation of machinery and equipment. Similarly, remote control systems heavily rely on low-latency communication to enable the effective operation of unmanned vehicles and remote-operated machinery from a distance.

Short-packet communication is recognized as an effective method to minimize communication latency, though it suffers from notable decoding errors with finite block lengths [2]. Non-orthogonal multiple access (NOMA) improves wireless system efficiency and capacity by allowing multiple users to simultaneously share the same spectral resources [3], thus increasing connection density and reducing latency. NOMA differentially allocates power to users to ensure fairness and minimize transmission conflicts, making it suitable for integrating with short-packet communication to address the IoT's low-latency demands. [4] introduced NOMA into short-packet communication, aiming to leverage the advantages to meet the low-latency requirements of the IoT era.

In recent years, movable antennas (MAs) have garnered significant attention due to their sufficient utilization of spatial degrees of freedom (DoFs) [5], which further enhances the performance of wireless communication systems. [6] introduces a fluid antenna-assisted multi-user downlink system, optimizing positioning and beamforming to enhance performance and

minimize transmission power. [7] introduces movable antennas in MISO NOMA downlink systems, optimizing power allocation and antenna positioning to improve channel capacity. The implementation, mathematical modeling, and performance analysis of communication systems utilizing MAs are comprehensively detailed and analyzed in [8]. Meanwhile, [9] presented advanced multiple-input multiple-output (MIMO) system where MAs are adjusted to boost system capacity by reshaping the MIMO channel effectively. [10] showed that adjusting MAs optimally can significantly reduce the total transmit power in MA-enhanced multiple access systems by creating favorable channel conditions. Based on these works, we consider whether MA can be applied to NOMA short-packet communication via antenna position optimization to further amplify its advantages.

In this letter, we investigate a short-packet downlink transmission system with NOMA assisted by MAs, where an access point (AP) transmits information to two users, each equipped with an MA. Considering the decoding error probability due to finite block length, our objective is to maximize the effective rate of successful data reception for core user (CU) while ensuring reliable communication for edge user (EU), by optimizing the coordinates of the MAs and the power and rate allocations of the AP. We decompose the complex non-convex optimization problem into two subproblems. Using successive convex approximation (SCA) technique, we obtain a local optimal solution for the first subproblem. Detailed steps for resolving the second subproblem are provided. Numerical results demonstrate that our proposed solution significantly enhances the effective rate of successful data reception for core user compared to NOMA short-packet communication with fixed position antennas (FPAs).

II. SYSTEM MODEL AND PROBLEM FORMULATION

In Fig. 1, an AP transmits information to two users simultaneously within the same frequency band using finite block lengths, where AP is equipped with a FPA, while each user is equipped with a MA capable of movement within a square region of side length A . The coordinates of u_i 's MA can be represented as $\mathbf{u}_i = [x_i, y_i]^T$, $-\frac{A}{2} \leq x_i, y_i \leq \frac{A}{2}$, where $i \in \{1, 2\}$. Here, the user with better communication conditions, characterized by higher channel gains, is denoted as u_1 , while the other user is denoted as u_2 . We assume that the channel model adopted is based on the far-field response. This implies that although MA are deployed at the user terminal, the angle-of-departure (AoD), the angle-of-arrival (AoA), and the amplitude of the complex coefficient of each channel path remain unchanged [8].

X. He, W. Chen, Q. Wu, and X. Zhu are with the Department of Electronic Engineering, Shanghai Jiao Tong University, Shanghai 200240, China (email: euphoria_0428@sjtu.edu.cn; wenchen@sjtu.edu.cn; qingqingwu@sjtu.edu.cn; xushengzhu@sjtu.edu.cn).

N. Cheng is with the School of Telecommunications Engineering, Xidian University, Xi'an 710071, China (e-mail: nancheng@xidian.edu.cn).

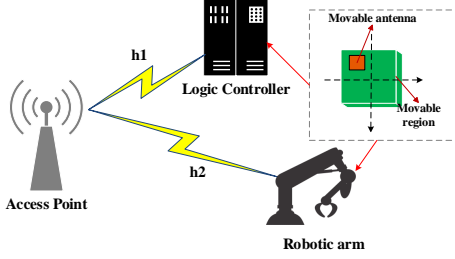


Fig. 1. System model diagram. In an actual intelligent factory automation communication system, an AP, a logic controller, and a robotic arm can be considered the smallest communication unit.

A. Channel Modeling

The mathematical expression for the signal received by the user u_i is given by

$$y_i = h_i x + n_i, i \in \{1, 2\} \quad (1)$$

where x is the input of the downlink transmission and $h_i \in \mathbb{N}$ is the channel coefficient from the AP to u_i . $x = \sqrt{P_1}x_1 + \sqrt{P_2}x_2$, where $x_1 \in \mathbb{C}$ and $x_2 \in \mathbb{C}$ represent the data symbols with unit power transmitted to two users. P_1 and P_2 represent the transmit powers allocated by the AP to u_1 and u_2 , respectively. The term n_i originates from the influence of the additive white Gaussian noise (AWGN) channel, $n_i \sim \mathcal{CN}(0, \sigma_i^2)$. h_i can be further decomposed into a product of several factors, as follows:

$$h_i = \mathbf{w}_i^H \mathbf{f}_i(\mathbf{u}_i). \quad (2)$$

The interpretation of the product term mentioned in the formula is as follows:

- $\mathbf{w}_i \in \mathbb{C}^{L_{i,r} \times 1}$ embodies the effective path response vector (EPRV) of u_i within the receive region.
- $\mathbf{f}_i(\mathbf{u}_i) = [e^{j\frac{2\pi}{\lambda} \mathbf{u}_i^T \boldsymbol{\rho}_{i,1}}, \dots, e^{j\frac{2\pi}{\lambda} \mathbf{u}_i^T \boldsymbol{\rho}_{i,L_{i,r}}}]^T \in \mathbb{C}^{L_{i,r} \times 1}$ is the field response vector (FRV) in the receive region of u_i , where the definition $\boldsymbol{\rho}_{i,k} \triangleq [\sin \theta_{i,k} \cos \phi_{i,k}, \cos \theta_{i,k}]^T$ holds. The elevation and azimuth angles of the u_i 's k -th receive path are denoted by $\theta_{i,k}$ and $\phi_{i,k}$, respectively, for $k = 1, 2, \dots, L_{i,r}$. Furthermore, λ is the wavelength.

B. Short-Packet NOMA Transmission

Applying successive interference cancellation (SIC) at the receiver to recover signals is an important aspect of NOMA [11]. Here, we assume that the upper bound of two users' channel gains satisfies the following relationship:

$$\|\mathbf{w}_1\|_1 > \|\mathbf{w}_2\|_1, \quad (3)$$

where the notation $\|\cdot\|_1$ denotes the l_1 norm. Taking fairness into consideration, NOMA strategies allocate a greater amount of power for communication with u_2 . Owing to this premise, u_1 can eliminate interference from u_2 through SIC. However, u_2 cannot eliminate interference from u_1 through SIC.

In short-packet communication, the decoding error probability at the receiver is non-negligible, primarily due to the finite block length [4]. We designate the effective decoding error probability at u_i as ϵ_i . According to [12], the decoding

error probability of x_2 at u_1 for a given transmission rate R_2 determined by AP, denoted by ϵ_2^1 , can be approximated by

$$\epsilon_2^1 \approx Q(f(\gamma_2^1, N, R_2)), \quad (4)$$

where Q-function is defined as $Q(x) \triangleq \frac{1}{\sqrt{2\pi}} \int_x^\infty \exp(-\frac{t^2}{2}) dt$. The computational expression for $f(\cdot)$ can be given by $f(x, y, z) = \ln 2 \sqrt{\frac{y}{1-(1+x)^{-z}}} (\log_2(1+x) - z)$, where N is the block length and γ_2^1 is the signal-to-inference-plus-noise (SINR) of x_2 at u_1 . In particular, γ_2^1 is given by

$$\gamma_2^1 = \frac{|h_1|^2 P_2}{|h_1|^2 P_1 + \sigma_1^2}. \quad (5)$$

Providing that SIC succeeds, the SNR of s_1 at u_1 and the decoding error probability of x_1 at u_1 can be written as

$$\gamma_1^1 = \frac{|h_1|^2 P_1}{\sigma_1^2}, \quad (6)$$

$$\epsilon_1^1 \approx Q(f(\gamma_1^1, N, R_1)). \quad (7)$$

If SIC does not succeed, the SINR of s_1 at u_1 and the decoding error probability of x_1 at u_1 can be calculated as

$$\gamma_1^{1'} = \frac{|h_1|^2 P_1}{|h_1|^2 P_2 + \sigma_1^2}, \quad (8)$$

$$\epsilon_1^{1'} \approx Q(f(\gamma_1^{1'}, N, R_1)), \quad (9)$$

where R_1 is the transmission rate determined by AP. The effective decoding error probability at u_1 is expressed by

$$\epsilon_1 = \begin{cases} \epsilon_1^1 (1 - \epsilon_2^1) + \epsilon_1^{1'} \epsilon_2^1, & R_1 \leq \log_2(1 + \gamma_1^{1'}), \\ \epsilon_1^1 (1 - \epsilon_2^1) + \epsilon_2^1, & \log_2(1 + \gamma_1^1) \leq R_1 \leq \log_2(1 + \gamma_1^{1'}). \end{cases} \quad (10)$$

The signal-to-inference-noise (SINR) of u_2 can be given by

$$\gamma_2^2 = \frac{|h_2|^2 P_2}{|h_2|^2 P_1 + \sigma_2^2}. \quad (11)$$

Then the effective decoding error probability of directly detecting x_2 at u_2 is given by

$$\epsilon_2 \approx Q(f(\gamma_2^2, N, R_2)). \quad (12)$$

Due to short-packet communication strategies, zero decoding error probability is unattainable, so effective throughput (bits per channel use) is used as the performance metric [4]. The effective throughput T_i for user u_i is given by

$$T_i = \frac{N_i}{N} R_i (1 - \epsilon_i), \quad (13)$$

where N_i represents the block length assigned to u_i and R_i signifies the transmission rate for u_i within the finite block length regime. Due to the absence of time division multiple access (TDMA) in NOMA transmission, it follows that $N_i = N$.

C. Problem Formulation

We aim to maximize the effective throughput of u_1 while constraining the maximum allocated power at the AP and ensuring communication reliability for u_2 (i.e., guaranteeing that the effective throughput of u_2 exceeds a certain threshold). Mathematically, the formulated optimization problem can be expressed as

$$\max_{\{R_1, R_2, P_1, P_2, \mathbf{u}_1, \mathbf{u}_2\}} T_1, \quad (14a)$$

$$\text{subject to } P_1 + P_2 \leq P_{max}, \quad (14b)$$

$$T_2 \geq T_0, \quad (14c)$$

$$\mathbf{u}_1, \mathbf{u}_2 \in \mathcal{C}, \quad (14d)$$

where $\mathcal{C} = \{[x_1, x_2]^T \mid -\frac{A}{2} < x_1, x_2 < \frac{A}{2}\}$. P_{max} denotes the average transmit power allocated by the AP within a block. T_0 represents the minimum effective throughput required to achieve reliable transmission for u_2 .

III. THE PROPOSED SOLUTION

Since optimization variables P_1, P_2, R_1 , and R_2 are independent of each other. In (14), the original optimization problem can be decomposed into two sets of optimization variables. To be specific, we can provide an expression for the channel gain, which is determined by the coordinates of the MAs as follows:

$$\begin{aligned} |h_i|^2 &= \mathbf{f}_i^H(\mathbf{u}_i) \mathbf{w}_i \mathbf{w}_i^H \mathbf{f}_i(\mathbf{u}_i) \\ &\triangleq \mathbf{f}_i^H(\mathbf{u}_i) \mathbf{W}_i \mathbf{f}_i(\mathbf{u}_i), i = 1, 2 \end{aligned} \quad (15)$$

where $\mathbf{W}_i \triangleq \mathbf{w}_i \mathbf{w}_i^H \in \mathbb{C}^{L_{i,r} \times L_{i,r}}$ denotes a constant positive semi-definite matrix. Since $|h_i|^2$ is highly non-concave with respect to \mathbf{u}_i and forming the feasible set from constraints (14c) is complicated, directly addressing Problem (14) poses considerable difficulty. Fortunately, channel gains for two users depend solely on the MA coordinates, affecting their own effective throughput individually. Our strategy entails decomposing the problem into two subproblems, which are more amenable to resolution, leveraging Proposition 1.

Proposition 1. *When other variables are given, the effective throughputs T_1 and T_2 are respectively monotonically increasing functions of the channel gain $|h_1|^2$ and $|h_2|^2$.*

Proof: The detailed proof is provided in Appendix. ■

Subproblem 1: Seek the optimal coordinates of the MAs to maximize the channel gain for users.

$$\max_{\{\mathbf{u}_1, \mathbf{u}_2\}} |h_i|^2 = \mathbf{f}_i^H(\mathbf{u}_i) \mathbf{W}_i \mathbf{f}_i(\mathbf{u}_i), \quad (16a)$$

$$\text{subject to } \mathbf{u}_i \in \mathcal{C}, \forall i \in \{1, 2\}, \quad (16b)$$

Subproblem 2: Seek the optimal resource allocation strategy at the AP under the condition of maximizing channel gain.

$$\max_{\{R_1, R_2, P_1, P_2\}} T_1, \quad (17a)$$

$$\text{subject to } P_1 + P_2 \leq P_{max}, \quad (17b)$$

$$T_2 \geq T_0, \quad (17c)$$

Subsequently, we will proceed to solve these two subproblems in the remaining part of Section III.

A. Solution to Subproblem 1

We employ SCA technique to address Subproblem 1, thereby obtaining the optimal values of the coordinates of the MAs [9]. Given any point \mathbf{u}_i^k within the feasible set, $\mathbf{f}_i(\mathbf{u}_i^k)$ is determined. Here, \mathbf{u}_i^k can serve as the point given in the k -th iteration of SCA. Then, the global lower bound can be provided by the following inequality:

$$\begin{aligned} |h_i|^2 &\geq \mathbf{f}_i^H(\mathbf{u}_i^k) \mathbf{W}_i \mathbf{f}_i(\mathbf{u}_i^k) \\ &\quad + 2\text{Re}\{\mathbf{f}_i^H(\mathbf{u}_i^k) \mathbf{W}_i (\mathbf{f}_i(\mathbf{u}_i) - \mathbf{f}_i(\mathbf{u}_i^k))\} \\ &= 2\text{Re}\{\mathbf{f}_i^H(\mathbf{u}_i^k) \mathbf{W}_i \mathbf{f}_i(\mathbf{u}_i)\} \\ &\quad - \mathbf{f}_i^H(\mathbf{u}_i^k) \mathbf{W}_i \mathbf{f}_i(\mathbf{u}_i^k). \end{aligned} \quad (18)$$

Without loss of generality, let us define $G(\mathbf{u}_i) \triangleq \text{Re}\{\mathbf{f}_i^H(\mathbf{u}_i^k) \mathbf{W}_i \mathbf{f}_i(\mathbf{u}_i)\}$.

After the aforementioned operations, $G(\mathbf{u}_i)$ is still not a concave function with respect to \mathbf{u}_i . Therefore, considering the ease of analysis when using a quadratic function as a surrogate to approximate the lower bound of the original function, we perform a second-order Taylor expansion of $G(\mathbf{u}_i)$ at \mathbf{u}_i^k , thereby obtaining a quadratic surrogate lower bound for it [9]:

$$\begin{aligned} G(\mathbf{u}_i) &\geq G(\mathbf{u}_i^k) + \nabla^T G(\mathbf{u}_i^k) (\mathbf{u}_i - \mathbf{u}_i^k) \\ &\quad - \frac{\delta_i^k}{2} (\mathbf{u}_i - \mathbf{u}_i^k)^T (\mathbf{u}_i - \mathbf{u}_i^k) \\ &= - \underbrace{\frac{\delta_i^k}{2} \mathbf{u}_i^T \mathbf{u}_i + (\nabla G(\mathbf{u}_i^k) + \delta_i^k \mathbf{u}_i^k)^T \mathbf{u}_i}_{\bar{G}(\mathbf{u}_i)} \\ &\quad + \underbrace{G(\mathbf{u}_i^k) - (\nabla G(\mathbf{u}_i^k) + \frac{\delta_i^k}{2} \mathbf{u}_i^k)^T \mathbf{u}_i^k}_{\text{constant}}. \end{aligned} \quad (19)$$

where $\nabla G(\mathbf{u}_i)$ denotes the gradient vector of $G(\mathbf{u}_i)$ over \mathbf{u}_i and δ_i^k is a positive number. After the aforementioned analysis, Subproblem 1 can be formulated as maximizing $\bar{G}(\mathbf{u}_i)$. The value of δ_i^k and the expression for $\nabla G(\mathbf{u}_i)$ are provided in the Appendix B. Due to the quadratic nature of $\bar{G}(\mathbf{u}_i)$ and the fact that the solution of the quadratic function can be expressed in closed form, the optimization problem for the k -th iteration of SCA can be given by

$$\max_{\mathbf{u}_1, \mathbf{u}_2} \bar{G}(\mathbf{u}_i), \quad (20a)$$

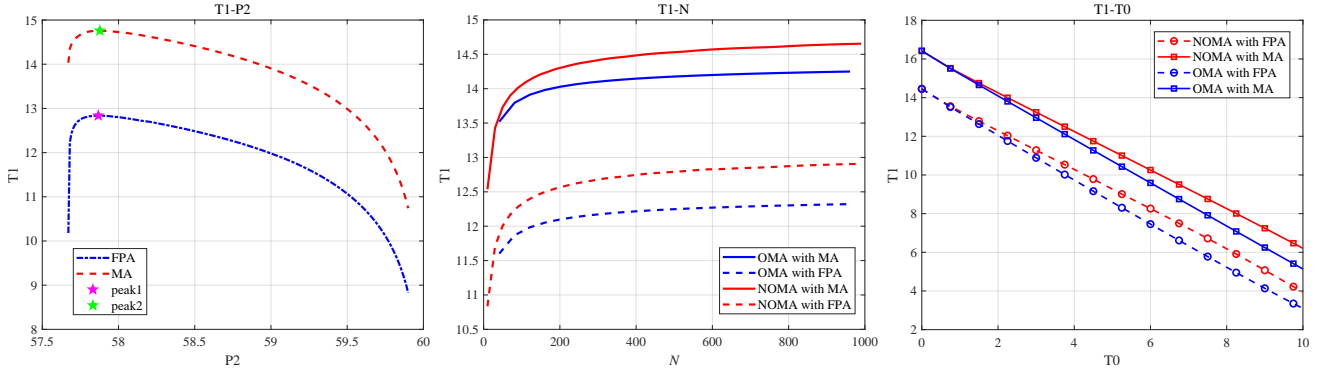
$$\text{subject to } \mathbf{u}_i \in \mathcal{C}, \forall i \in \{1, 2\}. \quad (20b)$$

The optimal $\mathbf{u}_i^{k+1,*}$ obtained from solving optimization problem (20) in the k -th iteration will be utilized for the subsequent iteration of SCA.

B. Solution to Subproblem 2

Here, we address Problem (17) as follows. Firstly, the equality $P_1 + P_2 = P_{max}$ is always guaranteed when maximizing T_1 subject to $T_2 \geq T_0$. Secondly, the equality $T_2 = T_0$ is always guaranteed when maximizing T_1 . Next, we provide an overview of the steps for solving Subproblem 2:

- *Step 1:* Given a feasible P_2 , since the value of T_2 is independent of R_1 and P_1 can be expressed as $P_{max} - P_2$,



(a) Graph of T_1 versus P_2 for $N = 100$ and $T_0 = 1$ bps/Hz.

(b) Graph of T_1 versus N for $T_0 = 2$ bps/Hz.

(c) Graph of T_1 versus T_0 for $N = 200$.

Fig. 2. Simulation results

we can utilize the equation $T_2 = T_0$ to solve for the desired R_2 . Here, a fixed-point iteration algorithm will be employed for the solution of R_2 (i.e., R_2^*):

$$R_2 := \frac{T_0}{1 - Q(f(\gamma_2^l, N, R_2))}. \quad (21)$$

To enforce Constraint (17c), P_2 is subject to a lower bound, which will be provided in the third step.

- *Step 2:* Now that P_1 , P_2 , and R_2 are all determined, we proceed to seek R_1 that maximizes T_1 . It can be given by

$$R_1^* = \begin{cases} R_1^\dagger, & \text{if } 0 \leq R_1 \leq \log_2(1 + \gamma_1^l), \\ R_1^\ddagger, & \text{if } \log_2(1 + \gamma_1^l) \leq R_1 \leq \log_2(1 + \gamma_1^h). \end{cases} \quad (22)$$

The values R_1^\dagger and R_1^\ddagger represent the roots of the equations $(1 - \epsilon_2^l)\mathcal{U}(\gamma_1^l, N, R_1^\dagger) + \epsilon_2^l\mathcal{U}(\gamma_1^h, N, R_1^\dagger) = 0$ and $\mathcal{U}(\gamma_1^l, N, R_1^\ddagger) = 0$ respectively. $\mathcal{U}(x, y, z)$ is defined as

$$\mathcal{U}(x, y, z) \triangleq 1 - Q(f(x, y, z)) - \frac{yz \ln 2}{\sqrt{2\pi(1 - (1+x)^{-2})}} e^{-\frac{f^2(x, y, z)}{2}}. \quad (23)$$

- *Step 3:* The content of the third step mainly provides the lower bound for P_2 . Assuming the lower bound for P_2 is P_2^l , then P_2^l is the root of the following equation:

$$R_2^\dagger(1 - Q(f(\gamma_2^l, N, R_2^\dagger))) = T_0. \quad (24)$$

The value R_2^\dagger represents the root of $\mathcal{U}(\gamma_2^l, N, R_2^\dagger) = 0$ and $\gamma_2^l = P_2^l |h_2|^2 / ((P_{max} - P_2^l) |h_2|^2 + \sigma_2^2)$.

- *Step 4:* The feasible set of P_2 is $P_2^l \leq P_2 \leq P_{max}$. Given that the feasible set of P_2 has been specified and is of finite length, we can employ linear search or golden section search to obtain the optimal value of P_2 , denoted as P_2^* . Then the optimal value of P_1 is $P_{max} - P_2^*$.

IV. NUMERICAL RESULTS

In this section, we present numerical results to validate the effectiveness of our MA-assisted short-packet downlink transmission with NOMA scheme by comparing it to a scheme

where MA is replaced by FPA. The distances between u_1 , u_2 , and the AP are set to 20 m and 60 m, respectively. Each user's noise power δ_i^2 is normalized, and the ratio of AP's average transmit power (P_{max}) to noise power is 60 dB. The movable region side length for MAs is $A = 3\lambda$, with initial MA positions at the origin, i.e., $\{\mathbf{u}_i\}_{i=1}^2 = [0, 0]^T$. Each user has 4 receive paths ($L_{i,r} = 4$). The EPRV of u_i is modeled as a circular symmetric complex Gaussian random vector, with n -th ($1 \leq n \leq L_{i,r}$) component $w_{i,n} \sim \mathcal{CN}(0, d_i^{-\alpha}/L_{i,r})$, where $\alpha = 1$ and d_i is the distance from u_i to the AP. Elevation and azimuth AoDs of each user are modeled as independent and identically distributed uniform distributions over $[0, \pi]$. The simulation results presented in this section were obtained by aggregating the outcomes of simulations with repetition counts on the order of 10^3 and subsequently computing their average.

In Fig. 2(a), We plotted the relationship between T_1 and P_2 , comparing our proposed scheme with the benchmark scheme, while optimizing the corresponding parameters (e.g., P_1, R_1, R_2) accordingly. In this figure, we first observe that our proposed scheme consistently outperforms the benchmark scheme in optimizing the effective throughput of u_1 regardless of the value of P_2 . We can find that the introduction of MA led to an approximately 16% improvement in the effective throughput of u_1 compared to the benchmark scheme. In fact, the maximum effective throughput of u_1 under the benchmark scheme serves as a lower bound for that under our proposed scheme.

In Fig. 2(b), we show that our proposed scheme achieves superior low-latency transmission by optimizing the effective throughput of u_1 for varying block lengths, compared to other schemes. With symbol duration T_s , the delay for a block length N is NT_s , indicating longer block lengths increase delay. Our scheme consistently outperforms the benchmark regardless of N . Notably, to achieve 13 bps/Hz, the benchmark requires nearly infinite block lengths, while our scheme achieves this with a block length under 100. In addition, within the experimental communication scenario, the superiority of NOMA over OMA in achieving low latency has been verified. Regardless of whether the users are equipped with MAs or FPAs, when the block length is fixed, the maximum throughput

achieved by u_1 employing NOMA is consistently higher than that achieved using OMA.

Fig. 2(c) depicts the variation of T_1 with respect to the constraint T_0 . Firstly, T_1 decreases as T_0 increases across different schemes. Secondly, the introduction of MA significantly enhances u_1 's effective throughput in both NOMA and OMA short-packet communications. Finally, when T_0 and T_1 are comparable in value, NOMA short-packet communication outperforms OMA in maximizing T1, with a more pronounced difference between the two.

V. CONCLUSION

In this letter, we investigated the MA-enhanced NOMA short-packet transmission performance for the downlink communication system. We focused on maximizing the effective throughput for the CU while ensuring the reliability of transmissions to the EU. This was done under the conditions of limiting the AP's average transmission power within a block, securing a minimum effective throughput for the EU, and confining the movable region of the MA for each user. Numerical results confirm that our proposed approach markedly improves the effective throughput for the CU, outperforming traditional NOMA short-packet communication systems with FPA.

APPENDIX A PROOF OF PROPOSITION 1

Combining (10), the effective throughputs T_1 and T_2 in (14) can be further expressed by the following equations:

$$T_1 = R_1(1 - \epsilon_1^1 + (\epsilon_1^1 - I)\epsilon_2^1), \quad (25)$$

$$T_2 = R_2(1 - \epsilon_2), \quad (26)$$

where I depends on the value of R_1 . If $R_1 \leq \log_2(1 + \gamma_1^1)$ holds, $I = \epsilon_1^1$, and if $\log_2(1 + \gamma_1^1) \leq R_1 \leq \log_2(1 + \gamma_1^1)$ holds, $I = 1$. According to [4], $Q(f(x, y, z))$ is a monotonically decreasing function with respect to x . Then, following (6) and (8) we have $\gamma_1^1 > \gamma_1^1$, which leads to $\epsilon_1^1 < \epsilon_1^1 \leq 1$ as per (7) and (9). Considering a function $g(x) = \frac{ax}{bx+c}$ with domain $x > 0$, where a , b , and c are all constants greater than zero, and its derivative with respect to x is $g'(x) = \frac{ac}{(bx+c)^2}$, it is evident that $g'(x)$ is greater than zero. Thus, $g(x)$ is a monotonically increasing function with respect to x . This implies that the SNR/SINR will increase as the channel gain increases as per (5), (6), (8) and (11).

Based on this, an increase in $|h_1|^2$ leads to increases in γ_2^1 and γ_1^1 , resulting in decreases in ϵ_2^1 and ϵ_1^1 . Given that $\epsilon_1^1 - I < 0$, we infer that $\frac{\partial T_1}{\partial \epsilon_1^1} < 0$, implying T_1 increases as ϵ_2^1 and ϵ_1^1 decrease. Similarly, an increase in $|h_2|^2$ raises γ_2^2 , decreases ϵ_2 , and thus increases T_2 as per (26).

APPENDIX B EXPRESSION FOR $\nabla G(\mathbf{u}_i)$ AND VALUE OF δ_i^k

In the k -th iteration of SCA, it is indispensable to compute the gradient vector of $G(\mathbf{u}_i)$ and δ_i^k . For analytical convenience, we introduce the following definitions:

$$\begin{aligned} \mathbf{v} &\triangleq \mathbf{W}_i \mathbf{f}_i(\mathbf{u}_i^k) \\ &= [b_1, \dots, b_l]^T = [|b_1| e^{j\angle b_1}, \dots, |b_l| e^{j\angle b_l}]^T \in \mathbb{C}^{l \times 1}, \end{aligned} \quad (27)$$

where $l = L_{i,r}$. Then $G(\mathbf{u}_i)$ can be further expressed as

$$\begin{aligned} G(\mathbf{u}_i) &= \text{Re}\{\mathbf{v}^H \mathbf{f}_i(\mathbf{u}_i)\} \\ &= \text{Re}\left\{ \sum_{p=1}^{L_{i,r}} |b_p| e^{j[\frac{2\pi}{\lambda}(x_i \sin \theta_{i,p} \cos \phi_{i,p} + y_i \cos \theta_{i,p}) - \angle b_p]} \right\} \\ &= \sum_{p=1}^{L_{i,r}} |b_p| \cos(\Gamma_p(\mathbf{u}_i)), \end{aligned} \quad (28)$$

where $\Gamma_p(\mathbf{u}_i) \triangleq \frac{2\pi}{\lambda}(x_i \sin \theta_{i,p} \cos \phi_{i,p} + y_i \cos \theta_{i,p}) - \angle b_p$. Subsequently, we can provide the expression for the gradient vector of $G(\mathbf{u}_i)$ with respect to \mathbf{u}_i :

$$\begin{aligned} \nabla G(\mathbf{u}_i) &= \left[\frac{\partial G(\mathbf{u}_i)}{\partial x_i}, \frac{\partial G(\mathbf{u}_i)}{\partial y_i} \right]^T \\ &= \begin{bmatrix} -\frac{2\pi}{\lambda} \sum_{p=1}^{L_{i,r}} |b_p| \sin \theta_{i,p} \cos \phi_{i,p} \sin(\Gamma_p(\mathbf{u}_i)) \\ -\frac{2\pi}{\lambda} \sum_{p=1}^{L_{i,r}} |b_p| \cos \theta_{i,p} \sin(\Gamma_p(\mathbf{u}_i)) \end{bmatrix} \end{aligned} \quad (29)$$

According to [9], we have $\delta_i^k \mathbf{I}_2 \succ \nabla^2 G(\mathbf{u}_i)$. After some manipulations, we have $\delta_i^k = \frac{8\pi^2}{\lambda^2} \sum_{p=1}^{L_{i,r}} |b_p|$.

REFERENCES

- [1] F. Hamidi-Sepehr *et al.*, "5G URLLC: Evolution of high-performance wireless networking for industrial automation," *IEEE Commun. Standards Mag.*, vol. 5, no. 2, pp. 132–140, Jun. 2021.
- [2] Q. Wu *et al.*, "A comprehensive overview on 5G-and-beyond networks with UAVs: From communications to sensing and intelligence," *IEEE J. Sel. Areas Commun.*, vol. 39, no. 10, pp. 2912–2945, Oct. 2021.
- [3] A. Ihsan, W. Chen, W. Khan, Q. Wu, and K. Wang, "Energy-efficient backscatter aided uplink NOMA roadside sensor communications under channel estimation errors," *IEEE Trans. Intell. Trans. Sys.*, vol. 24, no. 5, pp. 4962–4974, May. 2023.
- [4] X. Sun, S. Yan, N. Yang, Z. Ding, C. Shen, and Z. Zhong, "Short-packet downlink transmission with non-orthogonal multiple access," *IEEE Trans. Wireless Commun.*, vol. 17, no. 7, pp. 4550–4564, Jul. 2018.
- [5] H. Wang, Q. Wu, and W. Chen, "Movable antenna enabled interference network: Joint antenna position and beamforming design," *arXiv:2403.13573*, Available: <https://arxiv.org/abs/2403.13573>.
- [6] H. Qin, W. Chen, Z. Li, Q. Wu, N. Cheng, and F. Chen, "Antenna positioning and beamforming design for fluid antenna-assisted multi-user downlink communications," *IEEE Wireless Commun. Lett.* early access, Jan. 30, 2024, doi: [10.1109/LWC.2024.3360117](https://doi.org/10.1109/LWC.2024.3360117).
- [7] Y. Zhou, W. Chen, Q. Wu, X. Zhu, and N. Cheng, "Movable antenna empowered downlink NOMA systems: Power allocation and antenna position optimization," *arXiv:2405.18692*, Available: <https://arxiv.org/abs/2405.18692>.
- [8] L. Zhu, W. Ma, and R. Zhang, "Modeling and performance analysis for movable antenna enabled wireless communications," *IEEE Trans. Wireless Commun.* early access, Nov. 2023, doi: [10.1109/TWC.2023.3330887](https://doi.org/10.1109/TWC.2023.3330887).
- [9] W. Ma, L. Zhu, and R. Zhang, "MIMO capacity characterization for movable antenna systems," *IEEE Trans. Wireless Commun.*, vol. 23, no. 4, pp. 3392–3407, Apr. 2024.
- [10] L. Zhu, W. Ma, B. Ning, and R. Zhang, "Movable-antenna enhanced multiuser communication via antenna position optimization," *IEEE Trans. Wireless Commun.* early access, 2023, doi: [10.1109/TWC.2023.3338626](https://doi.org/10.1109/TWC.2023.3338626).
- [11] T. Cover, "Broadcast channels," *IEEE Trans. Inf. Theory*, vol. 18, no. 1, pp. 2–14, Jan. 1972.
- [12] Y. Polyanskiy, H. V. Poor, and S. Verdú, "Channel coding rate in the finite blocklength regime," *IEEE Trans. Inf. Theory*, vol. 56, no. 5, pp. 2307–2359, May 2010.